J Appl Electrochem (2012) 42:1049–1056
DOI 10.1007/s10800-012-0479-0

ORIGINAL PAPER

# Corrosion behavior of a duplex stainless steel under cyclic loading: a scanning Kelvin probe force microscopy (SKPFM) based microscopic study

**Tongyan Pan**

Received: 28 June 2012 / Accepted: 1 September 2012 / Published online: 7 September 2012


**Abstract** Corrosion fatigue behavior of the duplex stainless steel AISI 2205 was studied by the scanning Kelvin probe force microscopy (SKPFM) in the ambient temperature and pressure condition (25 °C, one standard atmospheric pressure). Surface-polished AISI 2205 samples were subject to a cyclic tensile stress while immersed in a 0.5 M NaCl solution. At specified time intervals, surface Volta potential of the samples was measured using the SKPFM in an oxygen and water regulated environment. The steel samples demonstrated a map of potentials with high contrasts between ferritic and austenitic grain domains, which was then linked to the actual corrosion potential (w.r.t. a saturated calomel electrode—SCE) based on a rigorous calibration procedure. The corrosion fatigue behavior of AISI 2205 was studied by comparing the SKPFM-measured Volta potentials of the same sample under applied cyclic strain and under no applied cyclic strain. It was found that AISI 2205 became more prone to corrosion when the applied tensile strain exceeds one percent (1 %).

**Keywords** Corrosion fatigue · Duplex stainless steel · Scanning Kelvin probe force microscopy

## 1 Introduction

The modern duplex steels possess good weldability, precise-controlled alloy contents that offer good resistance to local and uniform corrosion, and optimized microstructures contributing to high strength and high resistance to chloride stress corrosion cracking under many conditions [1]. Although the duplex stainless steel is relatively small among the overall stainless steel market, the duplex sector is becoming a fast-growing industry with strong prospects for continued growth as more industries start to value the overall life cycle costs. In addition to direct material savings, duplex steels can also generate longer life cycles and lower maintenance costs in many situations. According to the International Stainless Steel Forum (ISSF), the duplex production soared from 6,000 metric tons a month in 2004 to 10,000 metric tons by 2005 and reached 22,000 metric tons in 2008 [1, 2].

The early development of duplex steels in the 1930s featured the beneficial mechanical and physical properties of ferritic and austenitic steels, but with apparent limitations in the as-welded condition. Since the late 1960s and early 1970s, modern duplex grades have obtained significantly improved properties owing to several factors such as the introduction of vacuum and argon oxygen decarburization (VOD and AOD) processes that made it possible to achieve low carbon content in combination with high chromium content, high nitrogen content, and a favorable balance of ferrite and austenite [2]. These second-generation duplexes showed up in parallel with the offshore oil industry that required more versatile stainless steels to handle aggressive marine environments. While austenitic steels could also stand up to these aggressive environments, a nickel shortage at the time drove up their prices [1, 2].

Of the duplex steel family that includes mainly lean duplex, standard duplex, super duplex, and hyper duplex, the AISI 2205 (UNS S31803/32205) is the standard type that is known as the "workhorse" duplex steel and today accounts for over 80 % of the duplex market [3]. With approximately 50 % ferritic and 50 % austenitic phases, AISI 2205 was the first second-generation duplex steel

T. Pan (✉)
The Catholic University of America, 620 Michigan Avenue, N.E., Washington, DC 20064, USA
e-mail: pan@cua.edu

developed commercially in the mid-1970s [1, 4]. In general, AISI 2205 is known for its higher resistance against general corrosion than ferritic steels in many environments, superior yield strength that is nearly double that of austenitic steels, and improved resistance against stress corrosion cracking. Although the AISI 2205 stainless steel have demonstrated stronger resistance to stress-related corrosion problems than the ferritic and austenitic types, it is not completely exempt from such problems, particularly those by dynamic stresses that have been a potent destructive force and caused expensive infrastructure deterioration [5–9].

In the state of knowledge regarding stress-related corrosion of duplex steels, there exists a series of unsolved fundamental issues in spite of the abundant knowledge developed in the science of modern electrochemistry. Among these issues, the effect of cyclic tensile stress on the initiation of corrosion in the matrix of duplex steels is a well-known one. Regardless of the numerous studies conducted, the sub-microscale mechanism of such effect is still unclear [5–7]. So far many analyticochemical techniques have been used to investigate this critical process such as NMR and the X-ray based techniques (mainly X-ray reflectivity and X-ray diffraction) [10–12], considering the huge economic impact it implies. None of these methods, however, can effectively show the in situ electromotive potential map that further implies the locations of microscopic corrosion cells in steel. Instead, in the current state of practices regarding stress-related corrosion such as corrosion fatigue, the onset of corrosion is often assumed to occur randomly on the alloy surface, due to the missing of the sub-microscopic electrochemical information [6, 7].

The recent developments in the technology of scanning probe microscopy, particularly the scanning Kelvin probe force microscopy (SKPFM), have paved a new road for in situ exploration of the important early stage of corrosion fatigue at a resolution that has not been achieved before. SKPFM can measure the surface potential of the conductive samples, and today's commercial SKPFMs can readily reach an in-plane resolution of a few nanometers when operated in open air [13–17]. The surface potential mapped by SKPFM provides a clear contrast that allows the discerning of various metallurgical phases at the nanoscale and electrical potential as small as 1 mV. SKPFM enables microscopic potential measurements of various alloys even in air, which has showed great applicability based on correlations between SKPFM measurement and the actual in-electrolyte corrosion potential of the alloys [13, 14]. From this perspective, SKPFM is a promising tool for clarifying the sub-microscale mechanisms of corrosion in AISI 2205 stainless steel in relation to the acting cyclic tensile stresses.

Nevertheless, SKPFM measurement of surface potential must be performed with cautions as the Volta potentials can be easily disturbed by factors other than the local electrochemistry. Such factors usually include the structure and composition of passive oxidative film that can be instantly formed in air, and certain charged species adsorbed on the sample surface. At this standpoint, a careful correlation must be established between the Volta potential and the actual corrosion potential with all the aforementioned disturbances effectively controlled, which today can be readily achieved in an environment chamber such as a gas purification glovebox [18].

## 2 Theoretical background

The fundamental principle of SKPFM in measuring electrode potential is based on the concept of work function $\Phi$ of a metallic material or sample, which is defined as the minimum work required for extracting an electron from inside the sample (e.g., an electrode) to a position just outside the sample that is far enough to eliminate contributions from image forces (see Fig. 1a) [19]. Work function is equivalent to the difference in energy between the vacuum level and Fermi level indicated in Fig. 1a as $E^*_{vac}$ and $E_F$, respectively. Work function $\Phi$, therefore, consists of two parts per Eq. (1) for samples carrying no electrical charges, i.e., the chemical work $\mu_e$—the chemical energy needed to transfer the electron from the infinity into the sample, and the dipole or surface potential related work $e\chi$ that takes into account the electrostatic work to transport the electron through the dipole layer of sample surface, where $\chi$ is the potential drop between just inside the bulk material and just outside of it [20].

$$\Phi = -\mu_e + e\chi = -(\mu_e - e\chi) \tag{1}$$

For more general objects that carry electrical charges such as a SKPFM probe (Kelvin probe—KP in Fig. 1) and a metal/alloy sample in corrosion studies, an additional work term is needed to transfer the electron from just outside the sample surface to a position of absolute vacuum or infinitely far away (see Fig. 1b). The additional component can be calculated as $e\psi$, with which a generalized work function $\Phi^*$ can be defined per Eq. (2) as the work required for extracting an electron from within the sample (Point A in Fig. 1b) to infinitely far away, for example, Point B in Fig. 1b in the absolute vacuum. The symbol $\psi$ is the Volta potential which is equivalent to the potential drop from infinitely far away to a location just outside the surface.

$$\Phi^* = -\mu_e + e\chi + e\psi = -(\mu_e - e\chi - e\psi) \tag{2}$$

The sum of the dipole/surface potential $\chi$ and Volta potential $\psi$ gives the Galvani potential $\varphi$, which is the potential drop between the bulk sample and the vacuum level infinitely far away from the surface.

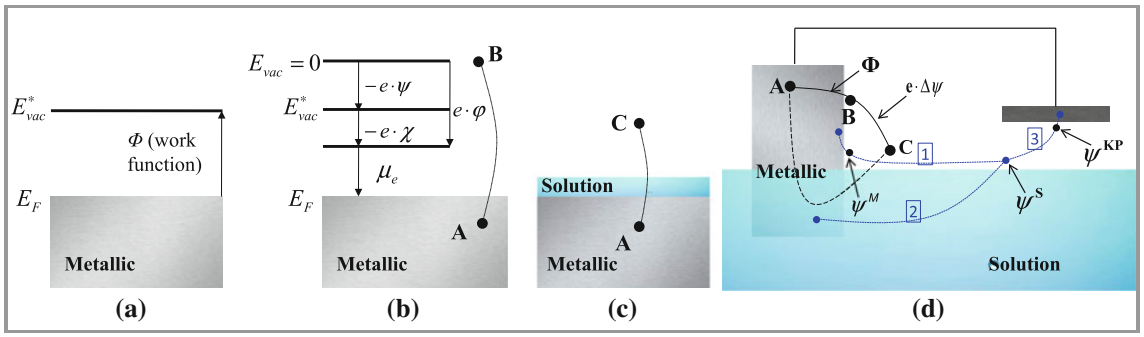


**Fig. 1** Schematic illustration of the working principles of SKPFM

$$\varphi = \chi + \psi \tag{3}$$

The absolute electrode potential $E_{abs}$ of a sample covered by a liquid layer (or an oxide film, an organic or polymer coating) (see Fig. 1c) can be defined, based on the concept of work function, as the minimum potential needed to transfer an electron from the Fermi level, through the metal/liquid (oxide or coating) interface (with the potential drop of $\Delta\varphi_M^{El}$), the liquid (oxide or coating) and its surface layer to a position just outside the liquid (oxide or coating) [19, 20]. $E_{abs}$ per Eq. (4) can be derived from Eq. (1) by adding an additional term $\Delta\varphi_M^{El} = \varphi_M - \varphi_{El}$, the potential drop at the metal/liquid (oxide or coating) interface (with "*El*" means "electrolyte"), and replacing the $\chi$ with the dipole/surface potential of the liquid (oxide or coating) surface $\chi_S$. $\Phi^*_{M-S}$ is the generalized work function of an electron that is transferred following the path A → C, i.e., from within the sample (e.g., an electrode) to a position outside the liquid (oxide or coating) layer covering the sample (see Fig. 1c) [20].

$$E_{abs} = \frac{1}{e}\Phi^*_{M-S} = \left(-\frac{\mu_e}{e} + \Delta\varphi_M^{El} + \chi_S\right) \tag{4}$$

According to Fig. 1d, if an electron is transferred following the path A → B → C instead of A → C, Eq. (5) is obtained, with $\psi^M$ and $\psi^S$ being the Volta potentials outside the metal and outside the liquid (oxide or coating).

$$E_{abs} = \frac{1}{e}\Phi + (\psi^M - \psi^S) \tag{5}$$

Based on the concept of absolute electrode potential, if a metallic SKPFM probe is connected to the sample by a metallic wire and positioned near the surface of the electrolyte as shown in Fig. 1d, Eq. (6) can be obtained corresponding to the three paths, considering that the work function difference between two points is a constant for a given situation. It is noted that the work required for an electron to transfer from the metal sample into the SKPFM probe (via the metallic wire) is negligible.

$$\begin{aligned} E_{abs} &= \frac{1}{e}\Phi^*_{M-S} = \left(-\frac{\mu_e}{e} + \Delta\varphi_M^{El} + \chi_S\right) \\ &= \frac{1}{e}\Phi^M + (\psi^M - \psi^S) = \frac{1}{e}\Phi^{KP} + (\psi^{KP} - \psi^S) \end{aligned} \tag{6}$$

The measurement of the Volta potential difference ($\psi^{KP} - \psi^S$) is what the SKPFM probe technique measures. In engineering practices, frequently it is not the value of the absolute electrode potential (or work function) of the probe tip but a relative electrode potential (or work function) of the tip measured w.r.t. a reference electrode, for example the standard hydrogen electrode, SCE, or Ag/AgCl electrode. The absolute electrode potential is related to the relative electrode potential or corrosion potential w.r.t. the standard hydrogen electrode by Eq. (7), where $E^0(H_2)_{\text{abs}}$ is the potential of the standard hydrogen electrode in the absolute electrode potential scale, which is a value between 4.44 and 4.85 V.

$$E_{cor-SHE} = E_{abs} - E^0(H_2)_{abs} \tag{7}$$

The electrode potential hence refers to the potential drop across the metal/liquid (oxide or coating) interface including the electrical double layer. As discussed before, the absolute electrode potential is not directly measurable and usually a reference electrode potential is measured w.r.t. a standard electrode. The electrode potential is frequently referred to as the open circuit potential or corrosion potential in practices.

The working mechanism of SKPFM is based on the implementation of the theoretical principles discussed above via the standard Atomic Force Microscopy [21, 22]. SKPFM operation involves first scanning the sample surface in the AFM tapping mode to determine the topography on a line-by-line basis, and then rescanning across the surface at a fixed height, i.e., in the "lift mode" with the metal-coated or doped silicon cantilever lifted to a fixed distance from the surface, typically 100 nm. The tapping piezo is turned off in the rescan, and an AC voltage $V_{ac}\sin(\omega t)$ is applied to the tip to stimulate oscillations of the cantilever [21, 22].

The AC voltage $V_{ac} \sin \omega t$ is connected to the Volta potential difference $\Delta\psi$ over the capacitor formed by the SKPFM cantilever/tip and the metallic sample. The magnitude of tip oscillations at the stimulating frequency $\omega$ is nulled on a point-by-point basis during the lift mode rescan by adding to the tip a DC voltage $V_{dc}$ that balances the Volta potential difference $\Delta\psi$. Accordingly, SKPFM nulls the first harmonic of the force exerted by an electric AC field on the charged cantilever/tip [21, 22]. The electric energy stored in the capacitor formed by tip/cantilever and sample is given in Eq. (8) in terms of its capacitance $C$ and the potential $V$ of the electrical field in the capacitor per Eq. (9) [21, 22].

$$W_{capacitor} = \frac{1}{2} V^2 C \tag{8}$$

$$V = \Delta\psi - V_{dc} + V_{ac} \sin(\omega t) \tag{9}$$

The electrical force in the capacitor can be obtained as the gradient of the potential $V$ per Eq. (10).

$$F_e = -\frac{dW_{capacitor}}{dz} = \frac{1}{2} V^2 \frac{dC}{dz} \tag{10}$$

Plugging Eq. (9) in Eq. (10) and considering the trigonometric relation: $sin^2(\omega t) = \frac{(1-cos(2\omega t))}{2}$, Eq. (10) eventually turns into Eq. (11) that forms the basis for the nulling mechanism in SKPFM, which is achieved by applying a DC voltage $V_{dc}$ equal to the Volta potential difference, i.e., $V_{dc} = \Delta\psi_{Sample}^{reference}$. Therefore, nulling of the force directly yields the measurement of Volta potential difference in SKPFM.

$$F_e = \frac{1}{2}\left(V_{dc} - \Delta\psi_{Sample}^{reference}\right)^2 \cdot \frac{dC}{dz} + \left(V_{dc} - \Delta\psi_{Sample}^{reference}\right) \cdot V_{ac} \sin(\omega t) \cdot \frac{dC}{dz} + \frac{1}{4}\left[V_{ac}^2 \cos(2\omega t) + V_{ac}^2\right] \cdot \frac{dC}{dz} \tag{11}$$

## 3 Experimental

The stainless steel AISI 2205 contains a high content of chromium but low content of carbon that helps minimize the precipitation chromium carbide due to welding and its susceptibility to intergranular corrosion. The chemical composition of AISI stainless steel 2205 studied in this study is given in Table 1. Since chromium stabilizes bcc ferrite that has marginal mechanical properties, nickel is added to make fcc austenite the preferred phase. AISI 2205 has a microstructure of approximately 50 % ferritic and 50 % austenitic phases, which gives the steel a higher strength than either ferritic or austenitic steels. AISI 2205 can be used in the "as-welded" condition even in severe corrosive conditions, and can be readily formed into different shapes.

In this study, AISI 2205 samples were tested using a Veeco SKPFM. The probe maps the surface Volta potential on the sample. The SKPFM probe used in this study had a conductive Pt/Ir-coated silicon tip with a resistivity of 0.01–0.025 Ω cm. The cantilever had a resonant frequency of 75 kHz, and the tips had an apex radius of 25 nm. These geometric characteristics were selected to ensure a good resolution in potential measurement.

Prior to SKPFM analysis, three steel samples (with two as duplicates) were prepared using a multi-stage mechano-chemical polishing with colloidal silica particles for 10 h. For the sample of 100 × 100 μm in size, the mechano-chemical polishing can ensure the surface roughness of one nanometer in the z direction [23]. A 0.5 M NaCl solution was prepared in which the steel samples were then immersed for the specified period of time. In order to simulate the realistic corrosion of stainless steel in damp air condition, the NaCl solution was left open to air when the steel sample was immersed in it so that oxygen from air had free access to the solution. A mechanical device was employed to apply a 1 Hz cyclic stress to the sample at two levels of strain: (1) 0.1 % tensile strain to ensure that the steel was within its elastic limit, and (2) 1 % tensile strain to generate some plastic deformation at which the steel's yield strength (launched at 0.2 % tensile strain) was exceeded. For a quick reference, the 500-time magnified microstructure of the steel sample (after the non-destructive SKPFM analyses) as made by electrolytic etching in an oxalic acid solution and scanning electron microscopy (SEM) graph are shown in Figs. 2a, b, respectively.

In order to get rid of the influence of NaCl solution (an electrolyte) on the distribution of surface potential as well as the influence of water molecules on the measurement of surface potential by SKPFM, the SKPFM analysis was conducted on the dry surface of the steel sample. However, as the steel surface also is sensitive to oxygen and water in air (to get surface passivated), the surface potential was measured in a glovebox regulated with nitrogen and argon gases to achieve an environment in which both water and oxygen were maintained below 1 ppm.

When it was time to take the readings of surface Volta potential, i.e., in 20, 40, and 60 min after an immersion period of 30 min in the NaCl solution, the sample was taken out of the NaCl solution, and dried and SKPFM-analyzed in the glovebox. The 30 min immersion period in the NaCl solution prior to SKPFM analysis was intended for the electrochemical reactions to reach equilibrium. In the SKPFM analyses, surface Volta potential was first taken on the unstressed sample; after that the same sample was returned to the NaCl solution and immediately stretched to 0.1 % tensile strain for the 20 and 40 min SKPFM analyses. After the 40 min analysis, the sample was stretched to the 1 % tensile strain and the surface potential was

**Table 1** Chemical composition of the AISI 2205 stainless steel in study

| AISI designation | Composition of alloying chemicals (wt%) | | | | | | | | |
|---|---|---|---|---|---|---|---|---|---|
| | C | Si | Mn | P | S | Cr | Mo | Ni | Others (*N*) |
| 2205 | 0.030 | 1.00 | 2.00 | 0.030 | 0.020 | 22.00 | 3.00 | 5.50 | 0.14 |

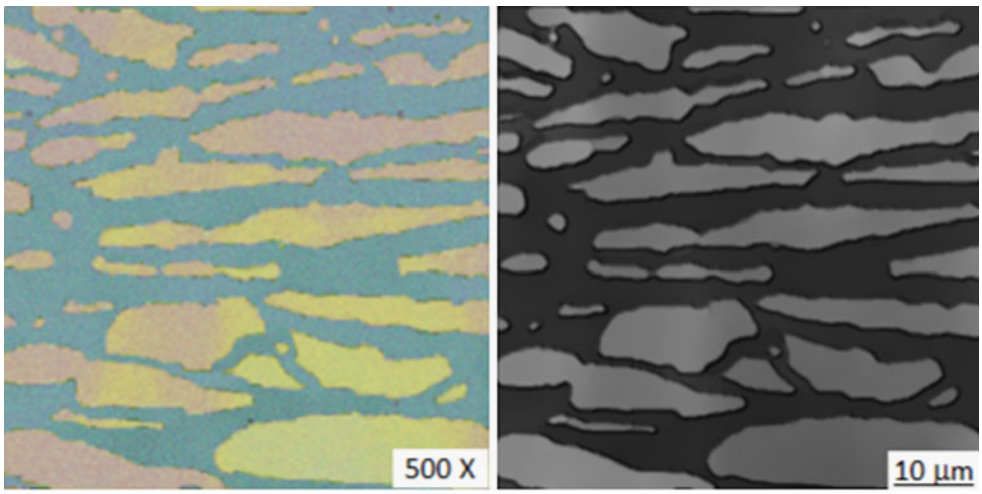


**Fig. 2** Microstructure of the stainless steel AISI 2205 **a** by electrolytic etching, **b** by SEM

measured after 20 more minutes, i.e., the 6 min, 1 % tensile strain analysis.

In order to make the SKPFM-based technology practically useful, the measured Volta potential needs to be correlated to the corrosion potential that usually is measured w.r.t. a standard electrode such as the saturated calomel electrode (SCE). Since the application of SCE is limited only to macroscopic measurements (on objects usually of above 1 cm sizes), a commercial high-purity electrolytic-type iron (99.95 % minimum purity) was adopted for the purpose of correlation. SKPFM-measured surface potentials of the high-purity iron samples were supposed to give small variation across the sample surface, which should be close to the average electrical potential or the corrosion potential of the sample measured w.r.t. SCE. NaCl solutions of nine different concentrations were prepared, from 0.1 to 0.9 M and incremented in 0.1 M, with one iron sample tested in each solution using both SKPFM and SCE. The 30 min surface Volta potential map of the steel was measured first in the 0.5 M NaCl solution.

The surface potential and corrosion potential of the other eight groups of iron samples, each with three duplicates and in one NaCl concentration, were also measured using the SKPFM and SCE, respectively. The average SKPFM result of each group was first converted to a Relative Surface Potential (RSP) by subtracting the average potential corresponding to the 0.5 M NaCl solution off the average SKPFM reading of the group. The high-purity iron sample in Fig. 3a demonstrates a relatively small range of surface potential, i.e., −6 to +5 mV in terms of RSP. The corrosion potential of the same iron sample was measured to be −229 mV w.r.t. the SCE electrode.

In order to establish the correlation between the SKPFM measured surface electrical potential (in terms of RSP) and the corrosion potential measured w.r.t. SCE, the nine RSPs were then correlated to the SCE results as shown in Fig. 3b. A definite linear relationship with a high correlation coefficient can be formulated between the RSPs and the SCE corrosion potentials. Fig. 3b essentially suggests the high validity and reliability of using SKPFM measured surface potential for evaluating the corrosion behavior of steels. Owing to the higher sensitivity of SKPFM, it gave measurements with higher variations than those w.r.t. the SCE as shown in Fig. 3b.

## 4 Results and discussion

In the state of knowledge regarding corrosion fatigue behavior of duplex stainless steel, the effect of cyclic tensile stress on the initiation of corrosion in stainless steels at the sub-microscale is still unclear. The SKPFM-measured surface Volta electrical potential is expected to shed light on the electromotive mechanisms for the formation of microscopic corrosion cells in the steel matrix. The 30 min surface Volta potential of the stainless steel sample in the

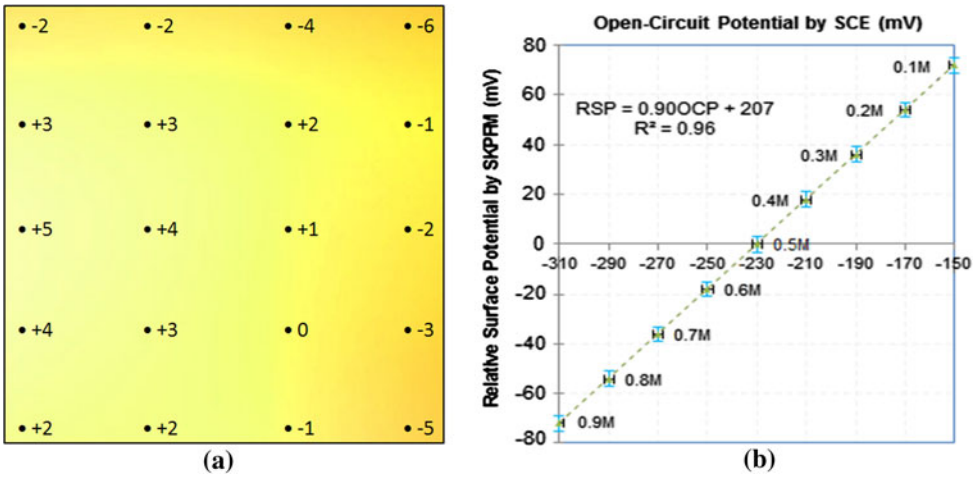


**Fig. 3** **a** 30 min RSP map (mV) of the high-purity iron sample in 0.5 M NaCl solution, **b** correlation between the 30 min RSP and SCE measured corrosion potential at different NaCl concentrations

0.5 M NaCl solution at the ambient temperature and atmospheric pressure is shown in Fig. 4a, which demonstrated a clear pattern with a distinct level of surface potential in the austenitic phase (yellow regions) from that in the ferritic phase (dark red regions). The RSP by SKPFM ranged between −26 mV (the darkest spot in Fig. 4a) and +1 mV (the brightest region in Fig. 4a).

As the AISI 2205 sample was subject to a 1 Hz, 0.1 % cyclic tensile strain in the horizontal direction for 20 more minutes while it was immersed in the 0.5 M NaCl solution, the surface potentials of most regions decreased to the range between −27 and −10 mV (see Fig. 4b); however the morphologies of the regions with different surface potentials did not obviously change, as compared to those in the unstressed sample (Fig. 4a). The slightly decreased upper bound in the austenitic regions and the more significantly decreased lower bound in the ferritic regions indicated that there was a non-uniform distribution of strain levels in the different grains of the steel sample. Obviously, the ferritic grains are stiffer than the austenitic ones as more elastic deformation and, therefore, more potential change occurs in the austenite phase. It is noteworthy that in Fig. 4b quite some locations at the austenite-ferrite interface (arrow-headed) show much darker regions than most ferritic regions other than such boundary locations, which essentially indicated even lower RSP at such locations.

In order to study the effect of strain level on the initiation of corrosion, after the execution of the first 20 min 1 Hz, 0.1 % cyclic strain the steel sample was maintained under the 0.1 % cyclic horizontal tensile strain and immersed in the 0.5 M NaCl solution for 20 more minutes. Figure 5a shows the surface potential map of the sample under the 0.1 % tensile strain after a total of 40 (20 + 20) min. It was obvious that the potential of most regions dropped slightly to between −30 and −11 mV, and no apparently further darkened area showed up in the sample. Observations made from Fig. 5a essentially tells that the sustained 0.1 % cyclic strain did not cause much change in the distribution of surface Volta potential once the steel became adapted to such cyclic strain, through elastic

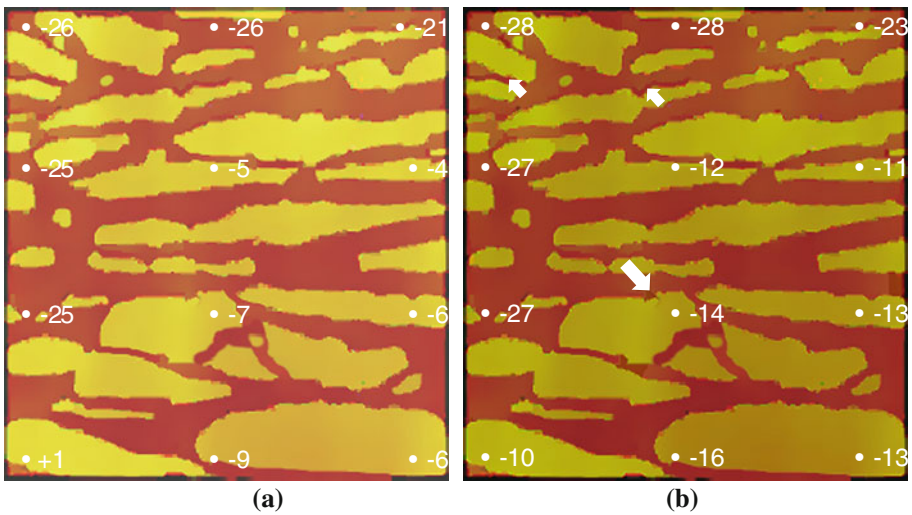


**Fig. 4** Surface potential map (mV) of AISI 2205 in 0.5 M NaCl solution **a** unstressed for 30 min, **b** under 1 Hz tensile strain (0.1 %) for 20 min

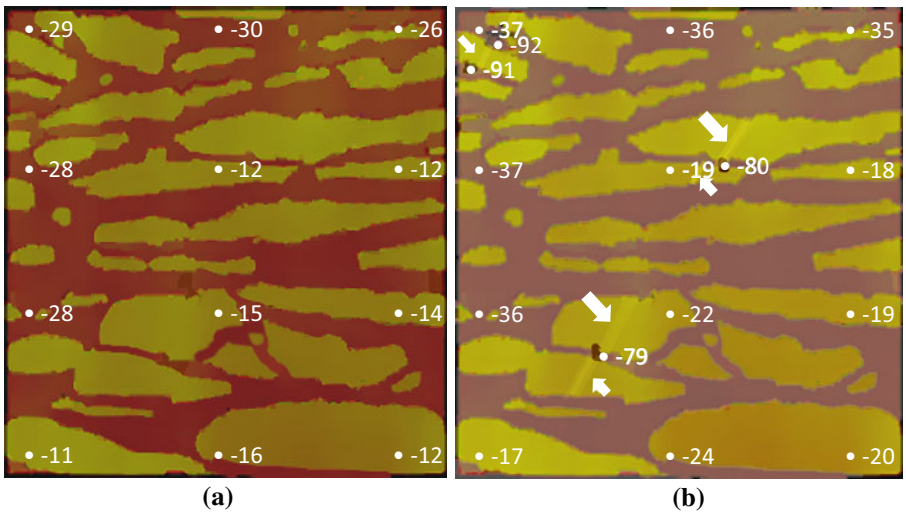


**Fig. 5** Surface potential map (mV) of AISI 2205 in 0.5 M NaCl solution **a** under 1 Hz tensile strain (0.1 %) for a total of 40 min, **b** under 1 Hz tensile strain (1 %) for 20 more minutes

position rearrangement among grains, after the first 20 min 1 Hz, 0.1 % cyclic strain [24–26].

After the 20 min execution of 1 Hz, 0.1 % cyclic strain, the same steel sample was switched to a one percent (1 %) cyclic horizontal tensile strain while still immersed in the 0.5 M NaCl solution. The 20 min RSP under the 1 % cyclic tensile strain per Fig. 5b showed significantly changed potential with obvious signs of localized corrosion. The Volta potential of most regions dropped to the range between −37 and −17 mV; and at some critical locations observed earlier in Fig. 4b active localized corrosion was initiated, where the RSP was significantly lower than other part of the region (−79 to −91 mV). Also, apparent slip bands in some austenitic grains can be seen (arrow-headed).

As to the mechanisms of the localized active corrosion shown in Fig. 5b, it seemed to be caused by the high strain and potential gradients that can be more easily launched at the interface of the slender ferritic grains and adjacent austenitic grains. Near the locations of the active corrosion, slip bands in austenitic grains usually also mean slip bands in the ferritic-austenitic interface, which may be of a different level due to the different deformation. Therefore, the different levels of deformation or strain among the three different phases, i.e., ferrite, austenite, and their interface zone might be the driving force of a potential gradient that eventually reached a high level to cause the formation of microscopic corrosion cells at the observed locations. Slip bands are the preferable sites of localized corrosion mainly because of the higher potential gradient that facilitates electron transfer at such locations, leading to corrosion. However, a more detailed explanation for the mechanisms of localized corrosion in matrix of duplex steels needs an even higher resolution study. Today with the availability of atomic-scale scanning Kelvin probe force microscopes, the atomic mechanisms of localized corrosion in steels can be readily studied, which is currently going on in the Corresponding Author's group.

## 5 Conclusions

In order to explore a new approach toward a fundamental understanding of the effect of dynamic tensile stress on the initiation of corrosion in the workhorse stainless steels: AISI 2205, the Conducting Atomic Force Microscopy was used to directly capture the potential differences among the different phases of the alloy. The surface potential of AISI 2205 samples was measured in the 0.5 M NaCl solution, based on which the corrosion behavior of the steel was studied through comparing the surface Volta potential under different strain levels. According to the analysis of the results from this experimental study, a series of findings are summarized as follows.

1. Conducting Atomic Force Microscopy is capable of providing a surface Volta potential map of steel surface at a sufficiently high lateral resolution and high sensitivity, which can be used to replace the existing standard or conventionally used electrochemical tools.
2. The surface Volta potential measured by SKPFM can be directly related to the actual corrosion potential of steels, and therefore can be used as a high-accuracy indicator to predict pitting or crevice corrosion of steels or other metals and alloys.
3. The surface Volta potential of stainless steel is more sensitive to plastic deformation/strain than to elastic deformation/strain in the steel matrix. Volta potential changes slightly in austenite and ferrite grains at 0.1 % strain. Above the 1 % strain, corrosion develops much faster.

4. Slip Bands are the preferable sites of localized corrosion due to the higher potential gradient that could facilitate electron transfer at such locations, leading to corrosion.
5. The use of glovebox is an effective way to minimize the water and oxygen induced passivation of steel surface.
6. High-resolution SKPFM points to a new direction for studying the atomic-level mechanisms of general corrosion related problems.

## References


1. IMOA (2009) Practical guidelines for the fabrication of duplex stainless steels, 2nd edn. International Molybdenum Association (IMOA), London
2. Alvarez-Armas I (2008) Duplex stainless steels: brief history and some recent alloys. Bentham Science Publishers Ltd, Havana, pp 51–57
3. ASM International (2008) ASM handbook vol.1: properties and selection: irons, steels, and high-performance alloys. American Society for Metals, Materials Park, pp 0002–44073
4. AISC (2011) Steel construction manual, 14th edn. American Institute of Steel Construction, Chicago
5. Jones DA (1996) Principles and prevention of corrosion. Prentice Hall, New Jersy
6. Graver DL (1985) Corrosion data survey—metals section, 6th edn. NACE, Kansas
7. Bagotsky VS (2005) Fundamentals of electrochemistry, 2nd edn. Wiley, New York. ISBN: 978-0-471-70058-6
8. Pan T, Nguyen T, Shi X (2008) Assessment of electrical injection of corrosion inhibitor for corrosion protection of reinforced concrete. J Transportation Res Board 2044:51–60
9. Pan T, Wang L (2011) Finite element analysis of chemical transport and reinforcement corrosion induced concrete cracking in variably saturated heterogeneous concrete. ASCE J Engg Mech 137(5):334–345
10. Growcock FB, Lopp VR (1988) The inhibition of steel corrosion in hydrochloric acid with 3-phenyl-2-propyn-1-ol. Corros Sci 28: 397–410
11. Pan T (2011) Quantum chemistry-based study of iron oxidation at the iron-water interface: an X-ray analysis aided study. Chem Phys Lett 511:315–321
12. Pan T, van Duin ACT (2011) Steel surface passivation at a typical ambient condition: atomistic modeling and X-ray diffraction/ reflectivity analyses. Electrocatalysis 2:307–316
13. Schmutz P, Frankel GS (1998) Characterization of AA 2024-T3 by scanning Kelvin probe force microscopy. J Electrochem Soc 145:2285
14. Schmutz P, Frankel GS (1998) Corrosion study of AA 2024-T3 by scanning Kelvin probe force microscopy and in situ atomic force microscopy scratching. J Electrochem Soc 145:2295
15. Guillaumin V, Schmutz P, Frankel GS (2001) Characterization of corrosion interfaces by the scanning Kelvin probe force microscopy technique. J Electrochem Soc 148:B163
16. Leblanc P, Frankel GS (2002) A study of corrosion and pitting initiation of AA2024-T3 using atomic force microscopy. J Electrochem Soc 149:B239
17. Muster TH, Hughes AE (2006) Applications and limitations of scanning Kelvin probe force microscopy for the surface analysis of aluminum alloys. J Electrochem Soc 153:B474–B485
18. Rohwerder M, Turcu F (2007) High-resolution Kelvin probe microscopy in corrosion science: scanning Kelvin probe force microscopy (SKPFM) versus classical scanning Kelvin probe (SKP). Electrochim Acta 53:290–299
19. Trasatti S (1991) Structure of the metal/electrolyte solution interface: new data for theory. Electrochim Acta 36(11–12):1659–1667
20. Trasatti S (1990) The 'absolute' electrode potential—the end of the story. Electrochimica Acta 35(1):269–271
21. Nonnenmacher M, O'Boyle MP, Wickramasinghe HK (1991) Kelvin probe force microscopy. Appl Phys Lett 58(25):2921–2923
22. Nonnenmacher M, Wolter O, Greschner J, Kassing R (1991) Scanning force microscopy with micromachined siliconsensors. J Vac Sci Technol B 9(2):1358–1362
23. Pan T, (2012) Stressed corrosion of an austenitic stainless steel studied by scanning Kelvin probe force microscopy. Anal Lett (DOI:10.1080/00032719.2012.694944)
24. Garcia C, de Tiedra MP, Blanco Y, Martin O, Martin F (2008) Intergranular corrosion of welded joints of austenitic stainless steels studied by using an electrochemical minicell. Corros Sci 50:2390–2397
25. Martin F, Hendriksen B, Katan A, Ratera I, Qi Y, Harteneck B, Liddle JA, Salmeron M (2011) Ultra-flat coplanar electrodes for controlled electrical contact of molecular films. Rev Sci Instrum 82:123901
26. Bertrand G, Rocca E, Savall C, Rapin C, Labrune J-C, Steinmetz P (2000) In situ electrochemical atomic force microscopy studies of aqueous corrosion and inhibition of copper. J Electroanal Chem 489:38–45